Analysis of the Impact of Land Use on Spatiotemporal Patterns of Surface Urban Heat Island in Rapid Urbanization, a Case Study of Shanghai, China

Hongyu Du [1],*, Fengqi Zhou [1], Chunlan Li [2,3], Wenbo Cai [4], Hong Jiang [5] and Yongli Cai [6],*

[1]   Institute of Ecology and Sustainable Development, Shanghai Academy of Social Sciences, No. 622, Middle Huaihai Road, Huangpu District, Shanghai 200020, China; zfq@sass.org.cn
[2]   Institute for Global Innovation and Development, East China Normal University, Shanghai 200062, China; 15598022233@163.com
[3]   School of Urban and Regional Sciences, East China Normal University, Shanghai 200241, China
[4]   Research Center for Eco-Environment Sciences, Chinese Academy of Sciences, Shuangqing Rd. 18, Beijing 100085, China; wbcai@rcees.ac.cn
[5]   Guizhou University of Traditional Chinese Medicine, Dong Qing South Road in Huaxi University, Gui'an New Area, Guiyang 550025, China; hongjll@126.com
[6]   School of Design, Shanghai Jiao Tong University, 800 Dongchuan RD. Minhang District, Shanghai 200240, China
*   Correspondence: duhongyu@sass.org.cn (H.D.); ylcai@geo.ecnu.edu.cn (Y.C.)

Abstract: In the trend of global warming and urbanization, frequent extreme weather influences the life of citizens seriously. Shanghai, as a typical mega-city in China that has been successful in urbanization, suffers seriously from the urban heat island (UHI) effect. The research concentrates on the spatial and temporal pattern of surface UHI and land use. Then, the relation between them are further discussed. The results show that for the last 15 years, the UHI effect of Shanghai has been increasing continuously in both intensity and area. The UHI extends from the city center toward the suburban area. Along with the year, the ratio in area of Agricultural Land (AL), Wetland (WL), and Bare Land (BL) has decreased. On the contrary, Construction Land (CL) and Green Land (GL) have increased. The average land surface temperature (LST) rankings for each research year from high to low were all CL, BL, GL, AL, and WL. CL contributed the most to the UHI effect, while WL and GL contributed the most to mitigate the UHI. The conclusion provides practical advice aimed to mitigate the UHI effect for urban planning authorities.

Keywords: land use; urban heat island; spatiotemporal patterns; Shanghai

1. Introduction

A deteriorating urban thermal environment is led by continuous urbanization and causes serial ecological consequences like expediting of photochemical smog [1,2] and extra energy consumption [3–6]. This threatens the health and life of citizens such as heat stroke and cardiac arrest [7,8], thus the research on the urban heat island (UHI) effect and its impact factors has become one of the focuses in recent decades [9–11], especially for mega-cities like Shanghai, China.

It has been well proven by previous research that urbanization is the driving factor of the UHI effect [12]. The main causes include the change of land use [13,14], the unique features of the airflow dynamics within the city [15] and artificial heat sources [16]. Among the main factors, the change of land use is the most critical [17–19]. Calculating the dependency of land surface temperature (LST) on land use reflects the relationship between society development and the environment. The results

will benefit the research on urban climate change [20] as there is already research in this field. It is proven that LST is significantly correlated with the fractional cover of vegetation (FV) and impervious surface area (ISA), which means that the spatial distribution of LST in regional scale can be explained by the variation of the two factors [21]. It was also concluded that LST is positively correlated with the normalized difference building index (NDBI), while negatively correlated with the normalized difference vegetation index (NDVI) and the normalized difference water index (NDWI) [22,23]. More quantitative study still needs to be carried out to better describe the relationship between LST and land use. This will benefit the solutions to a variety of problems related to urban climate change and its interaction with humans [24].

As a new technology invented in the recent decades, remote sensing (RS) has become one of the most effective methods to acquire LST data in large scale, real time, and continuous manner [25,26]. It overcomes the limitations of traditional meteorological station measurements and better supports the research of the urban thermal environment [27]. There is quite a lot of research in the field of thermal environment based on this method. Li et al. [28] applied RS data to explore the impact of land architecture on the LST and surface UHI in Phoenix, Arizona. Singh, Kikon, and Verma [18] assessed the negative impact of urbanization on the rising trend of temperature and degradation of urban ecology in Lucknow city over time with the help of Landsat data and field survey. Therefore, the RS method was applied in this research.

Although there is already research about the dependency of LST on land use throughout global cities, the government strategies in China are the most critical driving factor of urban development. The 2010 Shanghai Expo and the orientation to become the center of finance and shipment of the city changed the land use dramatically. How the factors impact the distribution and temporal dynamic of surface UHI during this rapid change is very interesting. Regarding this, the following basic problems still need to be addressed: what is the latest status of the summer surface UHI? How does the temporal and spatial pattern of surface UHI change with progressing urbanization? What are the strategical and historical driving factors for this? What is the advice for future urban planning to improve it?

This research aimed to solve the problems and direct the future planning of mega-cities with rapid development. The four results of the Landsat RS images shot under clear weather in summer from 2000 to 2015 were applied to present the dynamic change of surface UHI and land use of Shanghai in both a temporal and spatial manner. By analyzing the results, the LST dependency on urban land use will be revealed. Combined with urban planning data and history materials, the driving factors of the change will be discussed. The conclusions will provide advice and good reference for the future optimization of urban planning to improve the thermal environment.

2. Data and Methods

2.1. Study Area

Shanghai is one of the most developed cities in China. The city area has been expanding rapidly for the past two decades. During this period, dramatic changes of urban land use have taken place and cause serious urban thermal environment problems, especially in summer, which has gained the wide attention of the public. Thus, Shanghai is a typical example to proceed with research on the surface UHI dependency on the variation of land use during unorganized urbanization. Currently, the related research mainly concentrates on the day–night variation of the UHI pattern based on meteorological data and seasonal variation in the UHI pattern based on RS data [21,29,30]. It has already been proven that the UHI effect of Shanghai is stronger at night than during the day. Additionally, the UHI effect in autumn and winter is more obvious than in the other seasons [29,31]. Even so, in practice, the UHI effect in summer during the day influences the urban ecology the most as it usually makes high-temperature calamity even worse [32,33]. This leads to a calamity increase in both frequency and strength, together with the development of the city [34]. However, in order to provide hints for future city planning and

the mitigation of UHI, especially in summer daytime, the research on the temporal and spatial pattern of the surface UHI of Shanghai in summer still needs to be improved.

The city sits to the south of the Yangtze River estuary and in the middle portion of the east coast of China (Figure 1). It has 16 districts with a total area of 6340.5 km^2, a length of 120 km from north to south, and a width of 100 km from east to west.
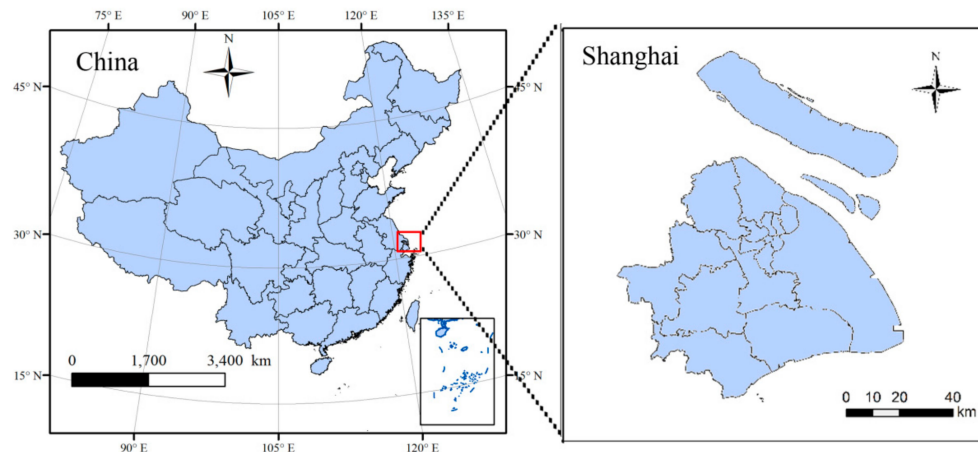

Figure 1. Location map of Shanghai, China.

The population expands continuously. By the end of 2015, the permanent resident population was 24.152 million including a census-registered population of 14.4297 million.

Shanghai has experienced rapid urbanization progress in the recent two decades, which can be shown in the data of subway construction and population growth (Table 1).

Table 1. The data source information of the remote sensing images.

Year	Subway Length	Population
2000	<30 km	16.09 million
2004	<100 km	18.35 million
2007	236 km	20.64 million
2015	617 km	24.15 million

Source: http://www.stats.gov.cn/.

2.2. Data Processing

In order to reduce the influences of weather and climate factors as much as possible, the RS images applied in this research needed to meet the two conditions below.

(1)　The thermal feature on the sampled dates are almost the same; and

(2)　On the day before the sampled day, the weather condition is stable (without strong wind or rain).

Condition 1 indicates that the thermal feature on the sampled date is almost the same while condition 2 indicates the accumulated historical influences are low. Actually, it is quite difficult to select the RS images because the requirements are very strict. The satellite has to pass the same location, at the same season, at a similar day time, under similar weather conditions, and with stable weather the day before. Finally, four images from 2000, 2004, 2007, and 2015 were selected rather than one shot every year. The weather conditions on the four sampled days and the days before them are shown in Table 2. The detailed RS data information is shown in Table 3.

Table 2. Weather conditions on the four sampled days and the days before them.

Date	Temperature	Wind Speed	Weather
2000.08.01	26–37	gentle breeze	Sunny
2000.07.31	28–35	gentle breeze	Sunny
2004.07.19	27–37	gentle breeze	Sunny
2004.07.18	29–36	light breeze	Sunny
2007.07.28	28–38	gentle breeze	Sunny
2007.07.27	29–37	gentle breeze	Sunny
2015.08.03	28–38	gentle breeze	Sunny
2015.08.02	29–38	light breeze	Sunny

Source: http://data.cma.cn/user/register/shareLevel/4.html.

Table 3. The data source information of RS images.

Satellite Sensor	Path/Row	Date
Landsat-7 ETM+	118/38, 118/39	2000.08.01
Landsat-5 TM	118/38, 118/39	2004.07.19
Landsat-5 TM	118/38, 118/39	2007.07.28
Landsat-8 OLI/TIRS	118/38, 118/39	2015.08.03

Source: http://glovis.usgs.gov/.

Except for the RS data, the following data were also used in this research.

(1) Google Earth high resolution images of Shanghai in 2000, 2004, 2007, and 2015. The images were used for the artificial abstraction of land use.

(2) The air temperature data from 10 meteorological stations on the same date as the RS images to verify the precision of the LST retrieval.

2.3. Research Methods

2.3.1. Land Surface Temperature Retrieval

The LST retrieval methods based on the infrared band of Landsat data include radiative Transfer equation (RTE), single channel method (SCM), and mono window algorithm (SWA). SWA eliminates the influence of error in the atmosphere simulation. However, the atmosphere parameters like average temperature and transmittance are normally difficult to acquire. The accuracy of SCM is highly influenced by the air humidity [35]. Shanghai is usually hot and wet in summer, so it is not appropriate to apply the SCM. According to the measured atmospheric profile, the RTE can reach an accuracy of 0.6 °C [36]. Therefore, in this research, the RTE method was applied to retrieve the LST of Shanghai in summer based on the new data from the thermal infrared sensor (TIRS) on the Landsat-8 satellites launched in February, 2013. ENVI 5.1 is a complete platform software tool for the processing of RS images [37] and was applied to preprocess the raw RS images. The process includes radiometric calibration, atmospheric correction, cutting, and splicing. During atmospheric correction, the atmospheric radiation was simulated based on the principle of the RTE by the model in MODTRAN 4.0, which is professional software for atmospheric correction. Through this simulation, the downward and upward atmospheric radiance $L_{atm,i}\downarrow$, $L_{atm,i}\uparrow$ and atmospheric transmissivity τ can be estimated. With the land surface emissivity ε, the $B(T_s)$ can then be obtained by Equation (1). Consequently, the LST T_s can be calculated by Equation (2).

$$L_{sensor,i} = \tau_i \varepsilon_i B(T_s) + (1 - \varepsilon_i)\tau_i L_{atm,i}\downarrow + L_{atm,i}\uparrow \tag{1}$$

$$B(T_s) = \frac{C_1}{\lambda^5\left(e^{(C_2/\lambda T_s)} - 1\right)} \tag{2}$$

Equation (1) is the RTE above-mentioned. $L_{sensor,i}$ is the radiation intensity (W·m^{-2}·sr^{-1}·μm^{-1}) of the wave band with index number *i* measured by the satellite sensor, which can be abstracted by the grayscale value of the raw images by Equation (3).

$$L_{sensor,i} = G \cdot QCAL + \Delta \tag{3}$$

In Equation (3), *QCAL* is the grayscale value, G is the value of gain in the wave band with index number *i*, while Δ is the deviation value in the wave band with index number *i*. For the two thermal infrared bands of Landsat-8, the value of gains and offsets were all identical with values of 0.0003342 and 0.1, respectively.

In Equation (2), $B(T_s)$ is the radiation intensity of the black body calculated by the Plank radiation function. C_1 and C_2 are the radiation constants with values of 1.19104356×108 W·m^{-2}·sr^{-1}·μm^4 and 1.4387685×104 μmK, respectively. λ is the wave length, the unit is μm. Equation (2) can be transferred to Equation (4).

$$T_s = \frac{K_2}{\ln(1 + K_1/B(T_s))} \tag{4}$$

In Equation (4), K_1 (unit mW·m^{-2}·sr^{-1}·μm^{-1}) and K_2 (unit K) are preset constants before the launch of the satellite. For TIRS data of Landsat-8, values of K_1 and K_2 are shown in Table 4.

Table 4. The value of K_1 and K_2.

	TIRS 1	TIRS 2	TM	ETM+
K_1	774.89	480.89	607.66	666.09
K_2	1321.08	1201.14	1260.56	1282.7

2.3.2. Validation of LST Retrieval

The result of LST retrieval was validated by comparing it to the measured data by meteorological stations. Figure 2 shows the comparison of the data in 2004. The results indicate that the temperature trends were the same. The difference is that the LST curve has a higher amplitude of vibration. This is caused by the land surface feature. At high temperature points, the lands are covered by impervious surfaces, which have a higher temperature than the air (Xujiahui Station). In contrast, low temperature points are usually covered by vegetation or water, which have a lower temperature than the air (Chongming Station). Therefore, the results of the LST retrieval were valid, and could be applied for the following analysis.
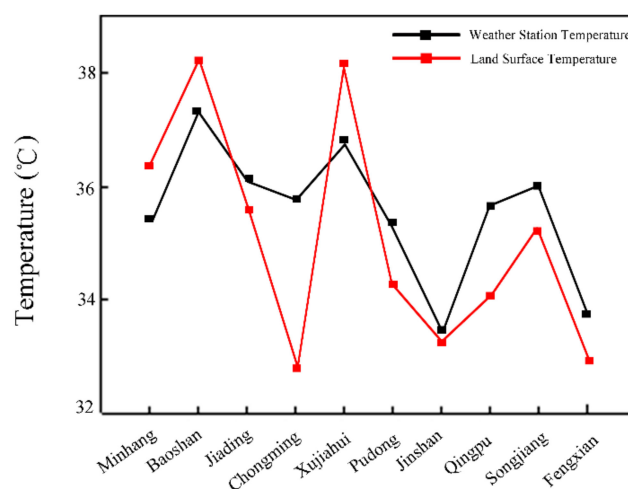

Figure 2. Retrieved land surface temperature compared to the meteorological station data.

2.3.3. Classification of LST

After retrieval, the LST was classified into seven types with the method of standard deviation classification. The calculation of the boundaries is shown in Equation (5). In this equation, *D* is the boundary of each type, *a* is times of 0.5 from 0–2.5, *X* is the average LST of the image, and the value s is the standard deviation. The seven types are listed in Table 5. The X and s for the four years were calculated separately.

$$D = X \pm a \times s \tag{5}$$

Table 5. The classification of the land surface temperature.

Temperature Grade	The Temperature Threshold
Extremely Low Temperature Zone (ELTZ)	$D \leq x - 2.5s$
Low Temperature Zone (LTZ)	$x - 2.5s < D \leq x - 1.5s$
Slightly Low Temperature Zone (SLTZ)	$x - 1.5s < D \leq x - 0.5s$
Medium Temperature Zone (MTZ)	$x - 0.5s < D \leq x + 0.5s$
Slightly High Temperature Zone (SHTZ)	$x + 0.5s < D \leq x + 1.5s$
High Temperature Zone (HTZ)	$x + 1.5s < D \leq x + 2.5s$
Extremely High Temperature Zone (EHTZ)	$D > x + 2.5s$

2.3.4. Calculation of UHI Intensity

UHI is defined as a higher temperature in the downtown than in suburban areas [38]. Therefore, the UHI intensity can be calculated as the temperature difference between them [39], which is defined in Equation (6).

$$UHII = LST_{urban} - LST_{suburban} \tag{6}$$

In this equation, LST_{urban} means the average LST in urban areas and $LST_{suburban}$ means the average LST in suburban areas

2.3.5. Classification of Land Use Type

The land use data, with a spatial resolution of 30 m, were obtained from RS images by supervised classification [40]. In order to improve the accuracy of the classification results, the land use data of Shanghai (Figure 3) from 2000, 2004, 2007, and 2015 were obtained through manual visual interpretation and corrected based on high-resolution Google Earth images. Field trips were also conducted when images could not clearly indicate land use. The land use was classified into five types: Constructive Land (CL), Green Land (GL), Wetland (WL), Agricultural Land (AL), and Bare Land (BL).
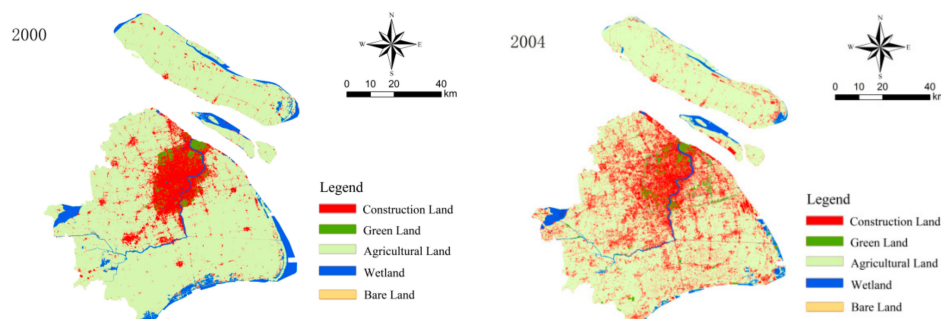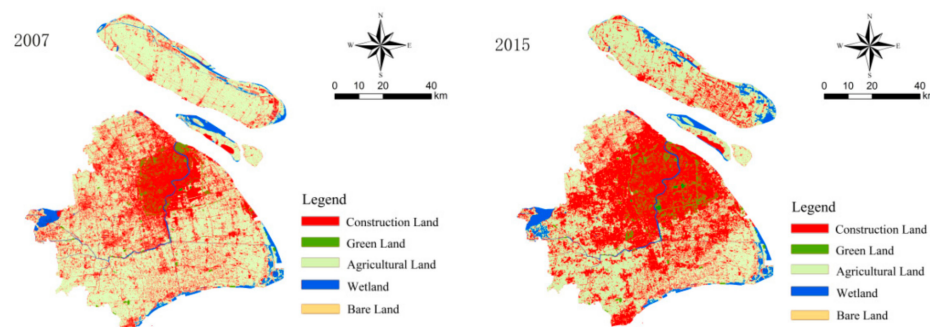

Figure 3. *Cont.*

Figure 3. The map of land use in different years.

3. Results

3.1. Spatial and Temporal Pattern of Urban Surface (UHI)

3.1.1. Spatial Distribution Characteristics of Urban Surface UHI

Figure 4 shows the result of LST classification of the four research years based on the data from the LST retrieval. The EHTZ had a scattered distribution in small areas, mainly the riparian of the Huangpu River and the industrial parks of Baoshan District. Most of the regions within the outer ring road and the central districts of satellite cities like Songjiang and Jiading are HTZ. The ELTZ and LTZ are distributed mainly in Huangpu River and the islands of Chongming, Hengsha, and Changxing.
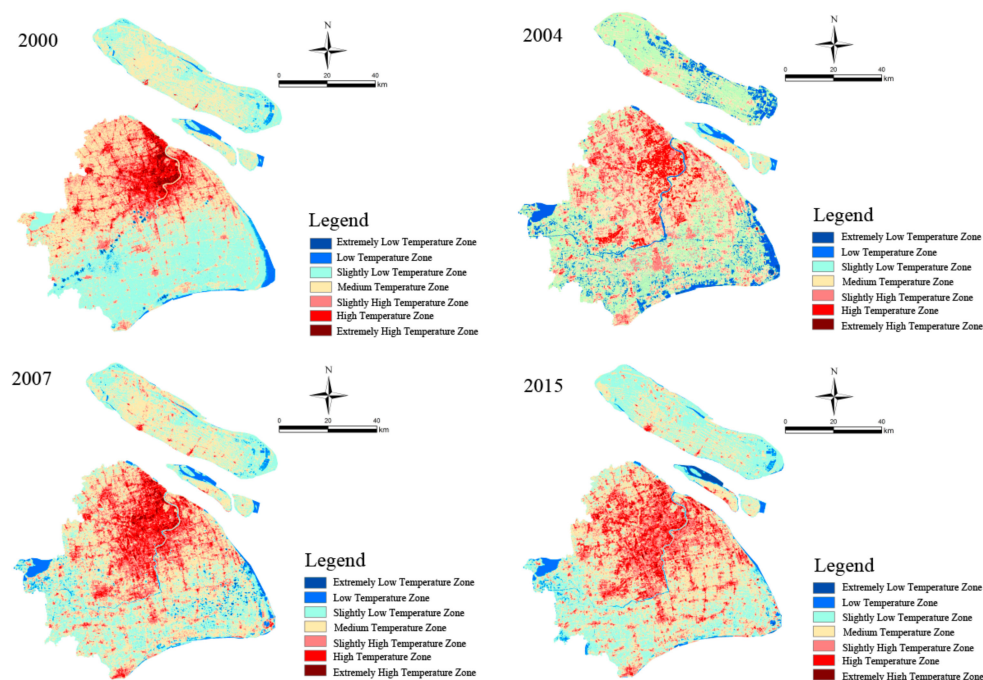
Figure 4. The classification of the land surface temperature in different years.

Figure 4 indicates that the total area of the HTZ and SHTZ is expanding, while the LTZ and SLTZ are shrinking with the year. In 2000, the summer UHI is distributed only in the northwest of the city. The area is the city downtown with a low greening rate, intensive buildings, and population. The coverage is mainly impervious surfaces. Compared to 2000, in 2004, the UHI downtown extended to the south where Minhang District is located. This area is one of the traditional bases of heavy industries with plenty of chemistry and ship factories beside the river. In 2007, the UHI expands even out of the outer ring road and radiated toward the suburban areas. Obvious hot spots appeared in the

center of suburban districts like Songjiang, Pudong, and Jiading. In 2015, almost half of the city was covered by middle or higher temperature zones. Only the Chongming, Fengxian, part of Qingpu, and Pudong (original Nanhui) Districts do not have large areas of UHIs, although hot spots already exist. The hot spots reflect further expansion of the UHI.

　　Cutting surface analysis can directly reflect the features of urban LST and its trend of changing. During the analysis, the selection of the cutting lines should be able to represent the overall features of the city. In this research, the lines are the meridian and parallel, which cross at the center of Shanghai: People Square. They stretch to the south, north, east, and west until the complete city is cut through (Figure 5). The meridian starts from the industrial blocks in Baoshan District, crosses the city center and Huangpu River, and finally reaches Fengxian District in the south. The parallel starts from the west of Qingpu District, crosses Jiading and the city center, and finally reaches Pudong District in the east. The LST distribution on the lines are shown in Figures 6 and 7.

Figure 5. The map of the profile location of the study area.

　　Figures 6 and 7 show that the LST trend on the meridian line was high in the north and low in the south in all years, while the LST trend on parallel line was high in the middle and low on both sides before 2007. This reflects that it passed through suburban area, urban areas, and then suburban areas again. The UHI effect trend is well shown on the waveform. After that, the LST curves on the parallel line become gentle.
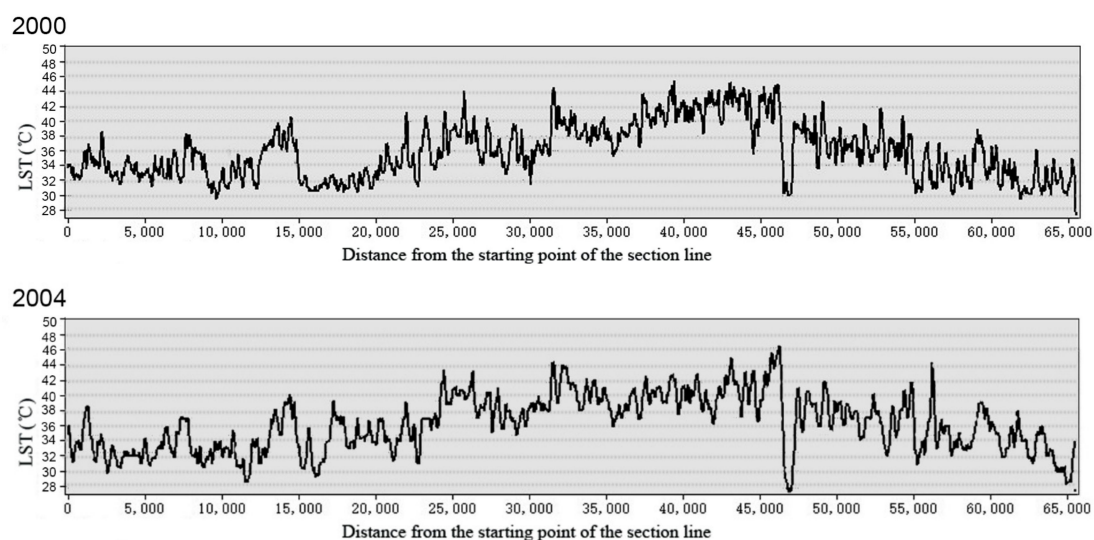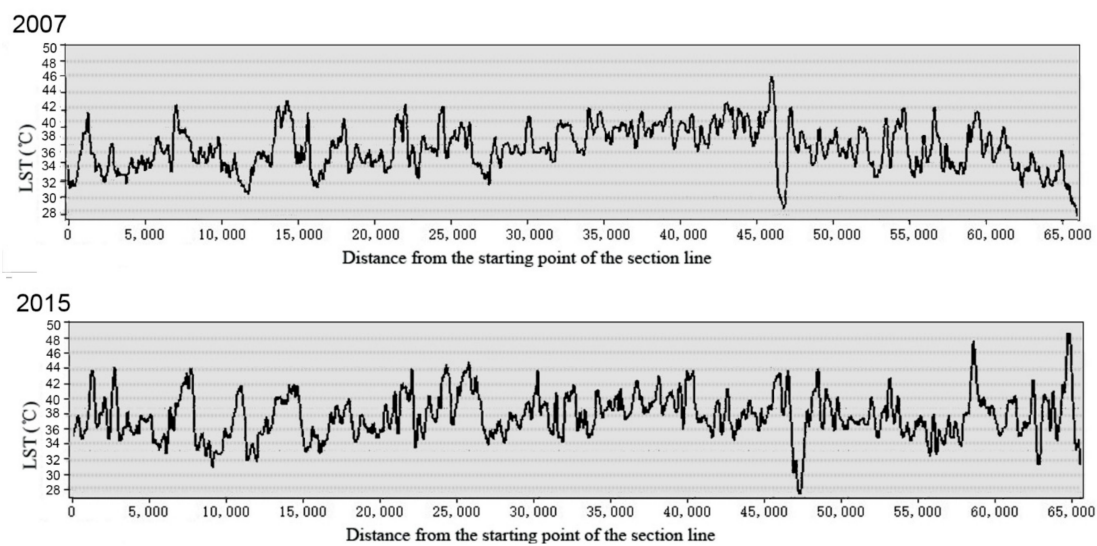

Figure 6. *Cont.*

Figure 6. The land surface temperature profile on the parallel from west to east.

In 2007 and 2015, the vibration on the parallel was sparser in frequency and lower in amplitude compared to 2000 and 2004. For the meridian line, the condition was similar; in 2015, the temperature waveform became sparser compared to 2000, 2004, and 2007. The amplitude of the vibrations decreased, which indicates a lower level of fragmentation in the underlying coverage.
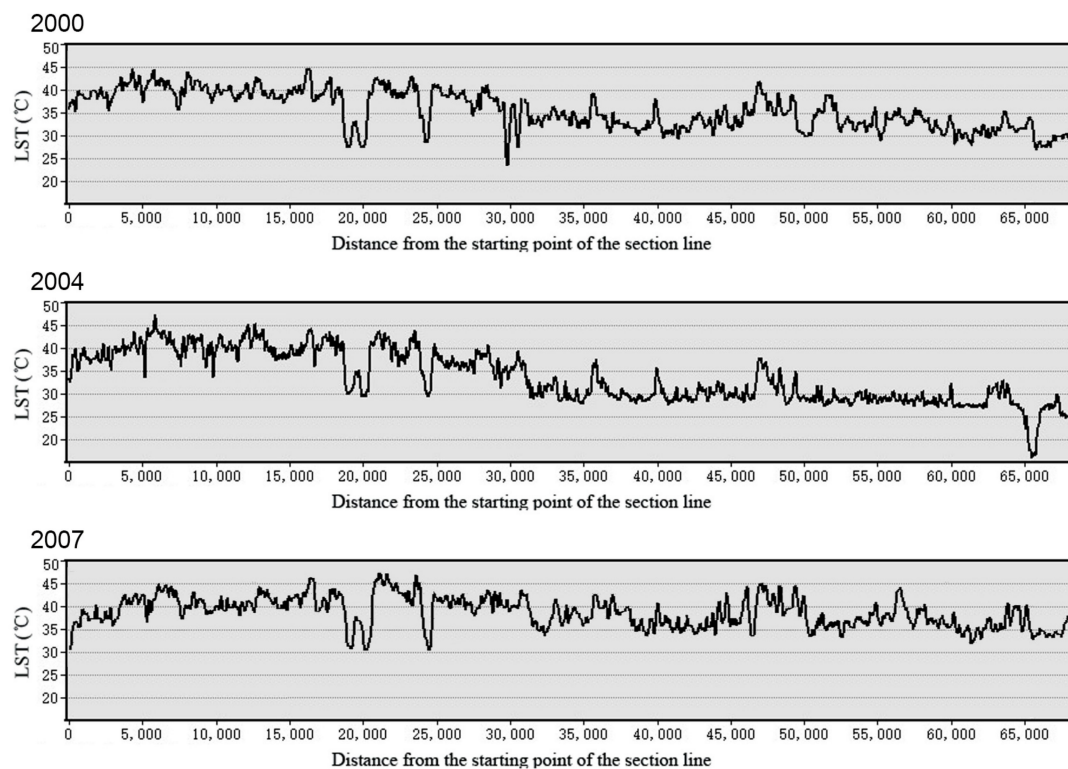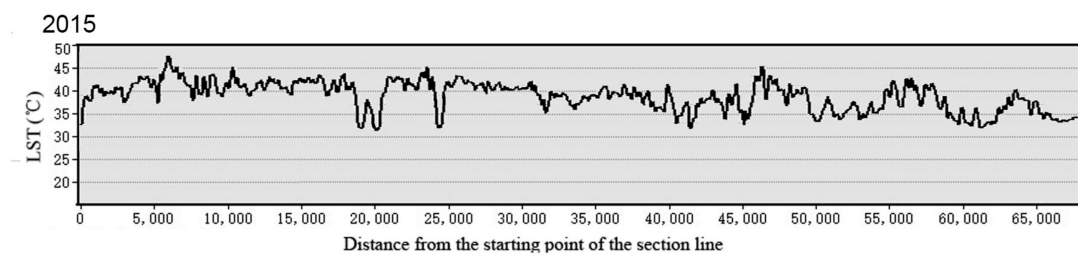

Figure 7. *Cont.*

Figure 7. The land surface temperature profile on the meridian from north to south.

3.1.2. Temporal Distribution Characteristics of Urban Surface UHI

Figure 8 and Table 6 indicate that the UHI in Shanghai increased continuously. It increased in intensity from 1.35 °C in 2000 to 2.86 °C in 2015 and in area rate from 8.56% in 2000 to 16.58% in 2015.
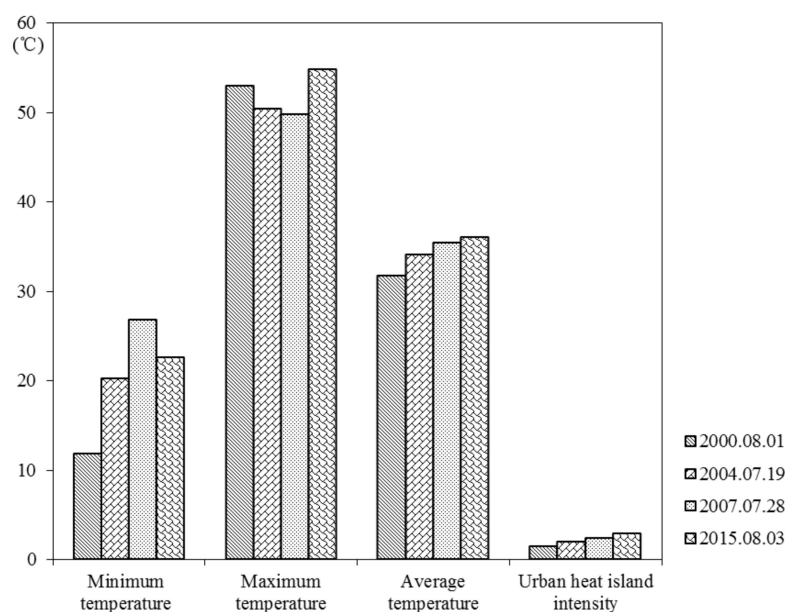

Figure 8. The land surface temperature and urban heat island intensity of the study area.

Table 6. The area ratio of each temperature area (%).

Temperature Grade	2000	2004	2007	2015	2000–2004 Annual Change	2004–2007 Annual Change	2007–2015 Annual Change
ELTZ	0.20	0.16	0.72	0.59	−0.04	0.56	−0.13
LTZ	3.55	2.79	2.83	1.40	−0.76	0.04	−1.43
SLTZ	31.64	31.17	30.73	16.14	−0.47	−0.04	−14.59
MTZ	40.71	40.17	39.02	36.48	−0.54	−1.15	−2.54
SHTZ	15.34	16.26	17.41	28.81	0.92	1.15	11.40
HTZ	7.24	8.13	8.03	14.44	0.91	−0.10	6.11
EHTZ	1.32	1.34	1.26	2.14	0.02	−0.08	0.88

According to Table 6, the ratio of the temperature zones changed significantly. The SLTZ, LTZ, and ELTZ decreased while the SHTZ, HTZ, and EHTZ increased. The maximum change in ratio happened in the SLTZ and SHTZ. Between 2007 and 2015, the ratio changes of SLTZ, LTZ, SHTZ, HTZ, and EHTZ were more significant than the other periods. This indicates that the intensity of the UHI in Shanghai increased rapidly between 2007 and 2015.

The SLTZ and ELTZ, which represent the cold island area, decreased in ratio with the year. The area ratio of LTZ decreased from 3.55% in 2007 to 1.99% in 2015. In contrast, the area ratio of HTZ

and EHTZ increased from 8.56% in 2000 to 9.47% in 2004. Although in 2007, the area ratio of HTZ and EHTZ decreased slightly to 9.29%, then increased dramatically in 2015 to 16.58%.

3.2. *Spatial and Temporal Pattern of Urban Underlying Surface*

3.2.1. Spatial Distribution Characteristics of Urban Underlying Surface

According to Table 7, AL, WL, and BL decreased in the ratio of area, and the number dropped from 37.95%, 25.19%, and 3.74% in 2000 to 21.71%, 12.36%, and 0.36%, respectively in 2015. The GL and CL increased in ratio with the year, the number increased from 7.815% and 25.31% in 2000 to 24.87% and 40.70% in 2015, respectively.

Table 7. The percentage of different land use types in different years.

Year	AL	GL	CL	BL	WL
2000	37.95	7.81	25.31	3.74	25.19
2004	35.15	12.00	29.14	1.68	24.03
2007	32.97	14.11	36.81	1.27	14.84
2015	21.71	24.87	40.70	0.36	12.36

According to Figure 2, compared to 2000, the land use in 2015 within the outer ring road of Shanghai has changed dramatically. There was massive new CL, while AL, WL, and BL decreased, and GL increased partially. In 2000, the urban GL was distributed mainly within the outer ring road. Among the districts, Changning, Xuhui, and Yangpu had higher vegetation coverage rates while Jing'an and Huangpu had low vegetation rates. The area of GL increased with the year. The GL outside the outer ring road was significantly larger than the inner ones. Baoshan, Minghang, and Pudong Districts had large areas of newly increased GL, while the Jinshan and Fengxian Districts had a small increase in GL. Regarding WL, the total area did not change much from 2000 to 2004. Except for the large WL distributed along the coast, Huangpu River, and Dianshan Lake, there were also plenty of WL intensively distributed inside the city. However, this condition changed in 2007, when massive WL were replaced by CL. This also happened to the mudflats beside the coast. A lot of WLs were changed into CL. In 2000, the CL was mostly within the outer ring road. In 2007, the CL was scattered distributed, with very few connected to each other. In 2015, continuous constructive districts were formed, so the expanding pattern of CL complies with the distribution change of SHTZ, HTZ, and EHTZ.

3.2.2. Temporal Distribution Characteristics of Urban Underlying Surface

To observe the spatial variation of land use in more detail, 20 annulus buffers with a width of 1 km were selected that covered a circle area with a radius of 20 km. Yuyuan Garden is the center of the circle (Figure 9). The ratio in area of each type of land use was calculated, which forms the curves. This indicates the variation of the ratio with the change of radius of the annulus buffers. Generally, the area within the outer ring road was from 0 to 16 km. The area from 16 to 20 km was outside of the outer ring road.

According to Figure 10, CL lay in the range of 0–16 km in 2000 and 2004, which means in the outer ring road. AL was distributed mainly in the range of 14–20 km, which was outside of the outer ring road. WL and GL were generally average distributed. The main portions of WL were the areas passed through by the Huangpu River. There were more GL within than outside of the outer ring road. Compared to 2004, the CL increased significantly in ratio from 2007 to 2015, and expanded toward the outside of the outer ring road. At the same time, especially in the range of 16–20 km, the AL decreased sharply. The WL outside the outer ring road decreased slightly, without significant change in distribution. There was a significant increase in the area of GL. The extra part was mainly distributed in the center of satellite cities. The data indicate that massive amounts of AL were transferred into

CL during the urbanization progress of Shanghai. The GL increased slightly due to awareness of its importance by the government.
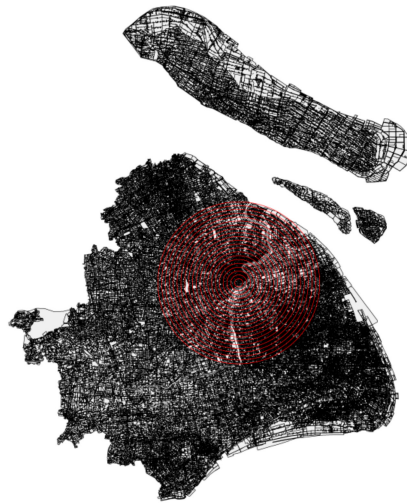

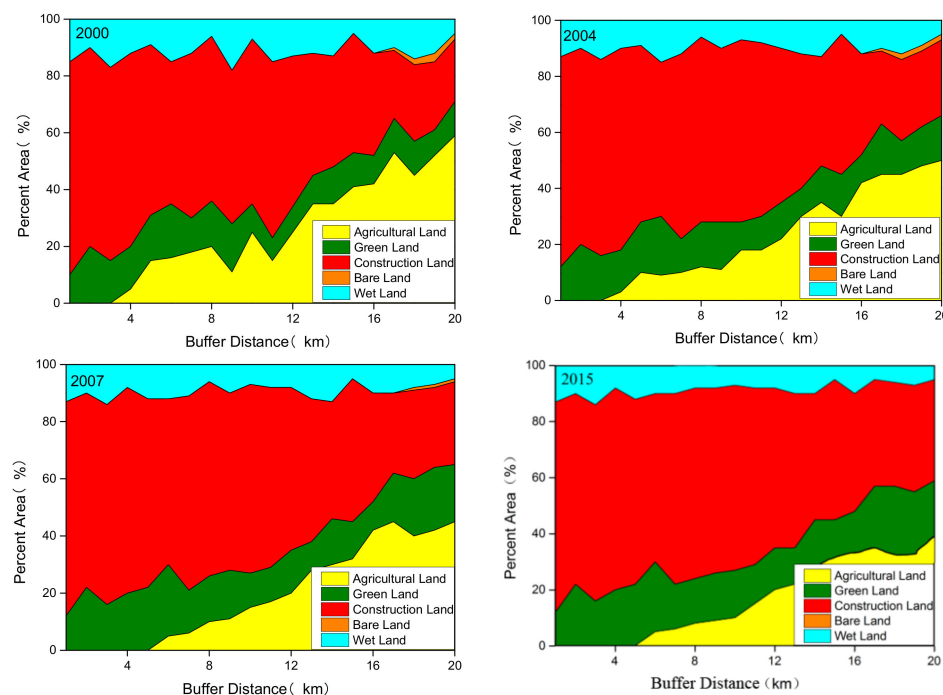**Figure 9.** The buffer ring from 0 to 20 km.

Figure 10. The change of the land use types area ratio with the buffer ring distance in different years.

3.3. Relation between the Dynamics of Urban LST and Underlying Surface

Different types of land use show different features of the absorbing and reflection rate of the solar radiation. The difference in thermal capacity also contributes to the variation of LST. By superimposing the retrieved LST over the result of land use classification, the temperature features of different land use types can be achieved, the results of which are shown in Figure 11.

According to Figure 11, the temperature features of different types of land use varied significantly. In the research years, the sequence of average summer LST rankings from the high to the low were all CL, BL, GL, AL and WL. Within the same year, AL, GL, and WL showed significantly lower LST than the average, while the average LST of CL and BL was significantly higher than the average.
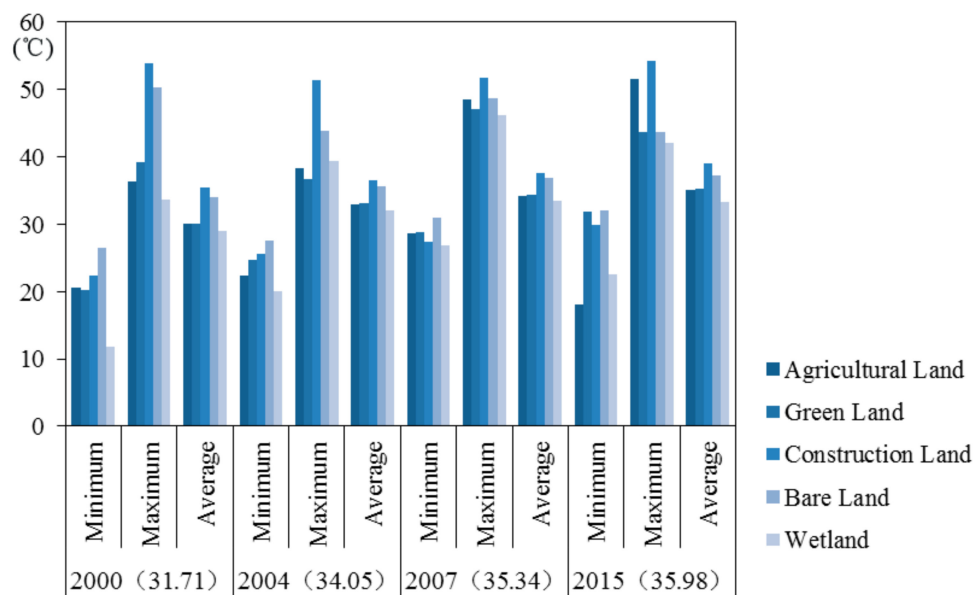
Figure 11. The land surface temperature of different land use in different years.

In order to better analyze the allocation of different temperature levels on the five types of land use, the spatial statistic function of ArcGIS was referred to in this research to calculate the ratio of different land use in each LST zone. The results are shown in Figure 12.
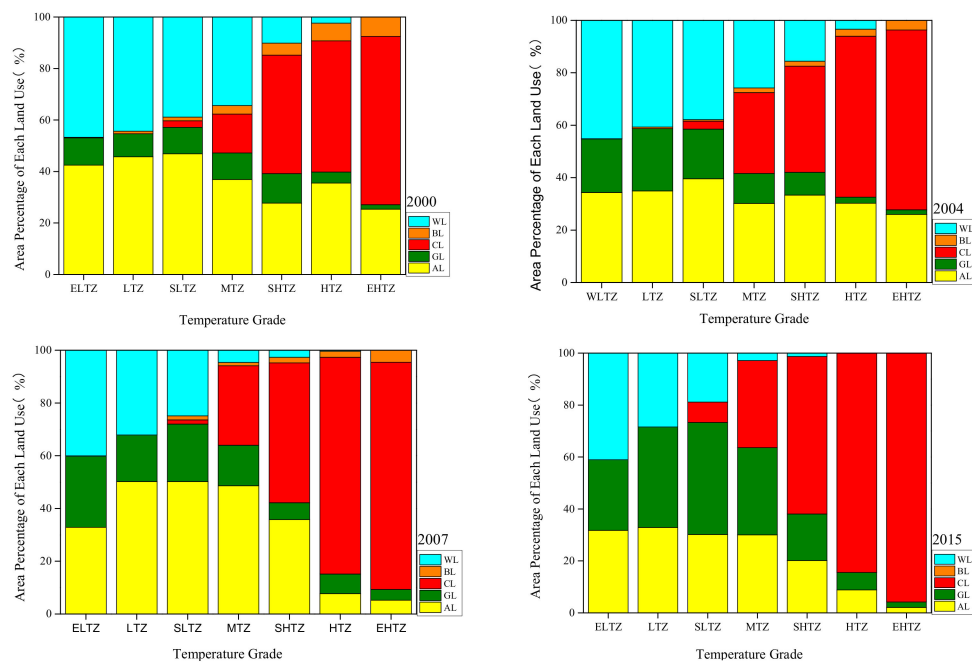

Figure 12. The area percentage of different land use types in each LST zone in different years.

According to Figure 12, the ratio of the five types of land use in different temperature zones were significantly different. However, the result of each year showed the same features. CL was the largest portion of EHTZ and HTZ. This indicates that CL contributes the most to the UHI effect. WL, GL, and AL was the largest part in SLTZ, LTZ, and ELTZ.

4. Discussion

4.1. The Relationship between Land Use and LST

The significant variation of the LST of different types of land use was mainly due to the features of their absorbing and reflection rates to solar radiation, thermal capacity, and moisture for evaporation. CL is usually covered by asphalt, bricks, and tiles, which have a strong absorbing rate of solar radiation [41]. The low thermal capacity makes the condition worse, which explains the reason why it has the highest LST. BL is mainly made of natural bare earth with high water permeability. Thus, it has a high thermal capacity and reflection rate of radiation heat. This makes BL have a lower LST than CL. GL is mainly covered by vegetation, which can make the LST of GL relatively low. AL has similar features as GL in the summer, however, this type of land use is distributed mainly in suburban areas where the background temperature is lower than the urban area. This makes the LST of AL slightly lower than GL [42]. Among the five types of land use, WL, which has a strong evapotranspiration effect, had the highest thermal capacity, thus had the largest temperature differences with the surrounding environment [43] and the LST was the lowest.

The above analyzed features well explained why the major land use of EHTZ was CL. In addition, the industrial activities produce massive artificial heat sources in the form of waste gas exhaust [44]. This makes the situation even worse, and finally, the EHTZ is formed. Similarly, covered mostly by building materials like asphalt, bricks, and tiles, the HTZ is formed by the low thermal capacity [45]. WL and AL had a significantly lower LST, thus ELTZ and LTZ were mostly covered by the two types of land use.

Therefore, the temporal and spatial pattern of urban LST is closely correlated with the type of land use, which is similar to the conclusion of Dissanayake, Morimoto, Ranagalage, and Murayama [19]. WL, GL, and AL have important contributions to dissipate urban heat and mitigate UHIs while CL had the greatest UHI effect.

4.2. The Relationship between LST and the Strategies of Urban Planning

Before 2007, because of the barrier effect of the Huangpu River, development was concentrated in the west riparian, and most of the CL was in the northwest of the city. The majority of suburban areas in the south consisted of agriculture and has developed continuously at a normal speed. The CL has not yet formed a continuous area but the fragmentation of the landscape is serious. This explains why the LST on the meridian cut line has a high trend in the north, is low in the south, and the LST on both the parallel and meridian vibrates.

Since 2007, in order to host the 2010 Expo, the government has grabbed the chance to invest in the construction of infrastructure like subways and expand the constructive areas of the city into previous suburban areas. The development of suburbs like Pudong and Jiading Districts has accelerated. Then, the urbanization level of suburban areas has risen significantly. Massive natural lands have been replaced by artificial surfaces and the fragmentation of land use has decreased. This is the reason why the LST vibrations in both Figures 6 and 7 become sparser in both frequency and amplitude on the parallel in the years 2007 and 2015. A similar trend was also seen in the meridian LST curve in 2015, where the frequency and amplitude became sparser because the UHI already covered continuous areas, which had small differences in land use and LST.

The government values the ecological functionality of urban GL, which has increased the total area of GL. However, since the total area is small compared to other types of land use, the cooling effect is limited. The urbanization process is mainly the result of AL transferring into CL, which makes the UHI effect more and more serious.

5. Conclusions

The research concentrated on the spatial and temporal distribution of LST and land use. Then, the relation between them were further discussed.

According to this research, the UHI effect of Shanghai has been increasing in both area and intensity for the past 15 years, together with the rapid urbanization of the city. The UHI extended from the downtown area in 2000 to even outside the outer ring road in 2015. As the years went by, the ratio in area of AL, WL, and BL decreased, while CL and GL increased. CL contributed the most to UHI while WL and GL contributed the most to mitigate UHI. The Shanghai Expo in 2010 has accelerated the urbanization since 2007, which has driven the most serious UHI increase between 2007–2015. In future, it is recommended to optimize the arrangement of urban functional areas and land use and increase WL and GL to improve the thermal environment and benefit the citizens.

Limited by the data availability, this research referred to only four RS images. Although the large weather conditions were controlled as much as possible to eliminate the influences from large scale climate, more concrete research needs to be further carried out. A combination of meteorological data and RS data or the introduction of RS data that covers the complete season can be a better method in further research. Furthermore statistical tests could be carried out to make the analysis more convincing. Except for land use, LST is also related to other factors such as human density and artificial heat sources, which are also interesting topics for future research.

References

1. Lai, L.-W.; Cheng, W.-L. Urban heat island and air pollution—An emerging role for hospital respiratory admissions in an urban area. *J. Environ. Heal.* **2010**, *72*, 32–36.
2. Zhong, S.; Qian, Y.; Zhao, C.; Leung, R.; Wang, H.; Yang, B.; Fan, J.; Yan, H.; Yang, X.-Q.; Liu, N. Urbanization-induced urban heat island and aerosol effects on climate extremes in the Yangtze River Delta region of China. *Atmos. Chem. Phys. Discuss.* **2017**, *17*, 5439–5457. [CrossRef]
3. Fung, W.; Lam, K.; Hung, W.; Pang, S.; Lee, Y. Impact of urban temperature on energy consumption of Hong Kong. *Energy* **2006**, *31*, 2623–2637. [CrossRef]
4. Kikegawa, Y.; Genchi, Y.; Kondo, H.; Hanaki, K. Impacts of city-block-scale countermeasures against urban heat-island phenomena upon a building's energy-consumption for air-conditioning. *Appl. Energy* **2006**, *83*, 649–668. [CrossRef]
5. Kolokotroni, M.; Giannitsaris, I.; Watkins, R. The effect of the London urban heat island on building summer cooling demand and night ventilation strategies. *Sol. Energy* **2006**, *80*, 383–392. [CrossRef]
6. Santamouris, M.; Cartalis, C.; Synnefa, A.; Kolokotsa, D. On the impact of urban heat island and global warming on the power demand and electricity consumption of buildings—A review. *Energy Build.* **2015**, *98*, 119–124. [CrossRef]
7. Tan, J.; Zheng, Y.; Tang, X.; Guo, C.; Li, L.; Song, G.; Zhen, X.; Yuan, D.; Kalkstein, A.J.; Li, F. The urban heat island and its impact on heat waves and human health in Shanghai. *Int. J. Biometeorol.* **2010**, *54*, 75–84. [CrossRef]
8. Shahmohamadi, P.; Che-Ani, A.; Etessam, I.; Maulud, K.; Tawil, N. Healthy Environment: The Need to Mitigate Urban Heat Island Effects on Human Health. *Procedia Eng.* **2011**, *20*, 61–70. [CrossRef]

9. Gao, L.; Yun, L.; Ren, Y.; Cui, Z.; Bi, H. Spatial and temporal change of landscape Pattern in the hilly-Gully region of loess Plateau. *Procedia Environ. Sci.* **2011**, *8*, 103–111.

10. Huang, J.; Pontius, R.G.; Li, Q.; Zhang, Y. Use of intensity analysis to link patterns with processes of land change from 1986 to 2007 in a coastal watershed of southeast China. *Appl. Geogr.* **2012**, *34*, 371–384. [CrossRef]

11. Kaza, N. The changing urban landscape of the continental United States. *Landsc. Urban Plan.* **2013**, *110*, 74–86. [CrossRef]

12. Renard, F.; Alonso, L.; Fitts, Y.; Hadjiosif, A.; Comby, J. Evaluation of the Effect of Urban Redevelopment on Surface Urban Heat Islands. *Remote Sens.* **2019**, *11*, 299. [CrossRef]

13. Tan, Z.; Lau, K.K.-L.; Ng, E. Urban tree design approaches for mitigating daytime urban heat island effects in a high-density urban environment. *Energy Build.* **2016**, *114*, 265–274. [CrossRef]

14. Wang, C.; Myint, S.W.; Wang, Z.; Song, J. Spatio-Temporal Modeling of the Urban Heat Island in the Phoenix Metropolitan Area: Land Use Change Implications. *Remote Sens.* **2016**, *8*, 185. [CrossRef]

15. Gago, E.; Roldán, J.; Pacheco-Torres, R.; Ordóñez, J. The city and urban heat islands: A review of strategies to mitigate adverse effects. *Renew. Sustain. Energy Rev.* **2013**, *25*, 749–758. [CrossRef]

16. Akbari, H.; Cartalis, C.; Kolokotsa, D.; Muscio, A.; Pisello, A.L.; Rossi, F.; Santamouris, M.; Synnefa, A.; Wong, N.H.; Zinzi, M. Local climate change and urban heat island mitigation techniques–the state of the art. *J. Civ. Eng. Manag.* **2016**, *22*, 1–16. [CrossRef]

17. Bokaie, M.; Zarkesh, M.K.; Arasteh, P.D.; Hosseini, A. Assessment of Urban Heat Island based on the relationship between land surface temperature and Land Use/ Land Cover in Tehran. *Sustain. Cities Soc.* **2016**, *23*, 94–104. [CrossRef]

18. Singh, P.; Kikon, N.; Verma, P. Impact of land use change and urbanization on urban heat island in Lucknow city, Central India. A remote sensing based estimate. *Sustain. Cities Soc.* **2017**, *32*, 100–114. [CrossRef]

19. Dissanayake, D.; Morimoto, T.; Ranagalage, M.; Murayama, Y. Land-Use/Land-Cover Changes and Their Impact on Surface Urban Heat Islands: Case Study of Kandy City, Sri Lanka. *Climate* **2019**, *7*, 99. [CrossRef]

20. Nastran, M.; Kobal, M.; Eler, K. Urban heat islands in relation to green land use in European cities. *Urban For. Urban Green.* **2019**, *37*, 33–41. [CrossRef]

21. Li, J.; Song, C.; Cao, L.; Zhu, F.; Meng, X.; Wu, J. Impacts of landscape structure on surface urban heat islands: A case study of Shanghai, China. *Remote Sens. Environ.* **2011**, *115*, 3249–3263. [CrossRef]

22. Guo, G.; Wu, Z.; Xiao, R.; Chen, Y.; Liu, X.; Zhang, X. Impacts of urban biophysical composition on land surface temperature in urban heat island clusters. *Landsc. Urban Plan.* **2015**, *135*, 1–10. [CrossRef]

23. Kikon, N.; Singh, P.; Singh, S.K.; Vyas, A. Assessment of urban heat islands (UHI) of Noida City, India using multi-temporal satellite data. *Sustain. Cities Soc.* **2016**, *22*, 19–28. [CrossRef]

24. Ramachandra, T.; Uttam, K. Land surface temperature with land cover dynamics: Multi-resolution, spatio-temporal data analysis of Greater Bangalore. *Int. J. Geoinformatics* **2009**, *5*, 44.

25. Wang, Y.; Berardi, U.; Akbari, H. Comparing the effects of urban heat island mitigation strategies for Toronto, Canada. *Energy Build.* **2016**, *114*, 2–19. [CrossRef]

26. Silva, J.S.; Da Silva, R.M.; Santos, C.A.G. Spatiotemporal impact of land use/land cover changes on urban heat islands: A case study of Paço do Lumiar, Brazil. *Build. Environ.* **2018**, *136*, 279–292. [CrossRef]

27. Rao, P.K. Remote sensing of urban "heat islands" from an environmental satellite. *Bull. Am. Meteorol. Soc.* **1972**, *53*, 647–648.

28. Li, X.; Li, W.; Middel, A.; Harlan, S.; Brazel, A.; Turner, B. Remote sensing of the surface urban heat island and land architecture in Phoenix, Arizona: Combined effects of land composition and configuration and cadastral–demographic–economic factors. *Remote. Sens. Environ.* **2016**, *174*, 233–243. [CrossRef]

29. Zhang, K.; Wang, R.; Shen, C.; Da, L. Temporal and spatial characteristics of the urban heat island during rapid urbanization in Shanghai, China. *Environ. Monit. Assess.* **2010**, *169*, 101–112. [CrossRef]

30. Zhang, H.; Qi, Z.-F.; Ye, X.-Y.; Cai, Y.-B.; Ma, W.-C.; Chen, M.-N. Analysis of land use/land cover change, population shift, and their effects on spatiotemporal patterns of urban heat islands in metropolitan Shanghai, China. *Appl. Geogr.* **2013**, *44*, 121–133. [CrossRef]

31. Li, J.-J.; Wang, X.-R.; Wang, X.-J.; Ma, W.-C.; Zhang, H. Remote sensing evaluation of urban heat island and its spatial pattern of the Shanghai metropolitan area, China. *Ecol. Complex.* **2009**, *6*, 413–420. [CrossRef]

32. Zhao, S.; Da, L.; Tang, Z.; Fang, H.; Song, K.; Fang, J. Ecological consequences of rapid urban expansion: Shanghai, China. *Front. Ecol. Environ.* **2006**, *4*, 341–346. [CrossRef]

33. Li, W.; Bai, Y.; Chen, Q.; He, K.; Ji, X.; Han, C. Discrepant impacts of land use and land cover on urban heat islands: A case study of Shanghai, China. *Ecol. Indic.* **2014**, *47*, 171–178. [CrossRef]

34. Zhao, M.; Cai, H.; Qiao, Z.; Xu, X. Influence of urban expansion on the urban heat island effect in Shanghai. *Int. J. Geogr. Inf. Sci.* **2016**, *30*, 1–21. [CrossRef]

35. Ding, F.; Xu, H. Sensitivity analysis of mono-window and single-channel algorithms to the possible errors in parameter estimation. *Sci. Surv. Mapp.* **2007**, *1*, 87–90.

36. Sobrino, J.A.; Jiménez-Muñoz, J.C.; Paolini, L. Land surface temperature retrieval from LANDSAT TM 5. *Remote. Sens. Environ.* **2004**, *90*, 434–440. [CrossRef]

37. Anbazhagan, S.; Paramasivam, C. Statistical correlation between land surface temperature (LST) and vegetation index (NDVI) using multi-temporal landsat TM data. *Int. J. Adv. Earth Sci. Eng.* **2016**, *5*, 333–346.

38. Oke, T.R. The energetic basis of the urban heat island. *Q. J. R. Meteorol. Soc.* **1982**, *108*, 1–24. [CrossRef]

39. Sun, Y.; Zhang, X.; Ren, G.; Zwiers, F.W.; Hu, T. Contribution of urbanization to warming in China. *Nat. Clim. Chang.* **2016**, *6*, 706–709. [CrossRef]

40. Du, H.; Ai, J.; Cai, Y.; Jiang, H.; Liu, P. Combined Effects of the Surface Urban Heat Island with Landscape Composition and Configuration Based on Remote Sensing: A Case Study of Shanghai, China. *Sustainability* **2019**, *11*, 2890. [CrossRef]

41. Taha, H. Urban climates and heat islands: albedo, evapotranspiration, and anthropogenic heat. *Energy Build.* **1997**, *25*, 99–103. [CrossRef]

42. Tan, C.L.; Tan, P.Y.; Wong, N.H.; Takasuna, H.; Kudo, T.; Takemasa, Y.; Lim, C.V.J.; Chua, H.X.V. Impact of soil and water retention characteristics on green roof thermal performance. *Energy Build.* **2017**, *152*, 830–842. [CrossRef]

43. Steeneveld, G.-J.; Koopmans, S.; Heusinkveld, B.; Theeuwes, N. Refreshing the role of open water surfaces on mitigating the maximum urban heat island effect. *Landsc. Urban Plan.* **2014**, *121*, 92–96. [CrossRef]

44. Yin, C.; Yuan, M.; Lu, Y.; Huang, Y.; Liu, Y. Effects of urban form on the urban heat island effect based on spatial regression model. *Sci. Total. Environ.* **2018**, *634*, 696–704. [CrossRef] [PubMed]

45. Mohajerani, A.; Bakaric, J.; Jeffrey-Bailey, T. The urban heat island effect, its causes, and mitigation, with reference to the thermal properties of asphalt concrete. *J. Environ. Manag.* **2017**, *197*, 522–538. [CrossRef] [PubMed]